Transcriptional Dysregulation in Postnatal Glutamatergic Progenitors Contributes to Closure of the Cortical Neurogenic Period

Vanessa Donega, Guillaume Marcy, Quentin Lo Giudice, Stefan Zweifel, Diane Angonin, Roberto Fiorelli, Djoher Nora Abrous, Sylvie Rival-Gervier, Muriel Koehl, Denis Jabaudon, et al.

Report

Cell Reports

Transcriptional Dysregulation in Postnatal Glutamatergic Progenitors Contributes to Closure of the Cortical Neurogenic Period

Graphical Abstract

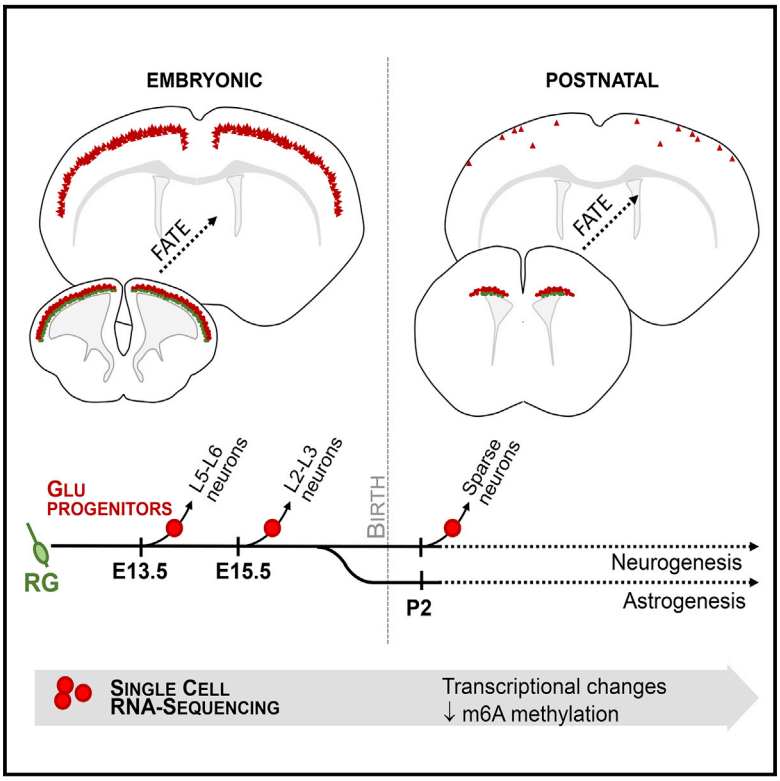

Highlights

- A large population of glutamatergic (Glu) progenitors persists in the postnatal SVZ
- Postnatal Glu progenitors arise from a persistent population of radial glial cells
- ScRNA-seq reveals transcriptional dysregulation in postnatal Glu progenitors
- Changes in m^{6}A methylation correlate with differentiation potential

Authors

Vanessa Donega, Guillaume Marcy, Quentin Lo Giudice, ..., Muriel Koehl, Denis Jabaudon, Olivier Raineteau

Correspondence

v.donega@umcutrecht.nl (V.D.), olivier.raineteau@inserm.fr (O.R.)

In Brief

Donega et al. revisit the closure of the corticogenesis period by showing that a large population of glutamatergic progenitors remains in the postnatal SVZ. They show a dysregulation of transcriptional programs, which parallels changes in m^{6}A methylation and correlates with a gradual decline in differentiation potential.

Donega et al., 2018, Cell Reports 22, 2567–2574
March 6, 2018
https://doi.org/10.1016/j.celrep.2018.02.030

CellPress

Cell Reports
Report

Transcriptional Dysregulation in Postnatal Glutamatergic Progenitors Contributes to Closure of the Cortical Neurogenic Period

Vanessa Donega,[1,*] Guillaume Marcy,[1,2] Quentin Lo Giudice,[1] Stefan Zweifel,[1] Diane Angonin,[1] Roberto Fiorelli,[3] Djoher Nora Abrous,[4,5] Sylvie Rival-Gervier,[6] Muriel Koehl,[4,5] Denis Jabaudon,[7] and Olivier Raineteau[1,3,8,*]
[1]Univ Lyon, Université Claude Bernard Lyon 1, Inserm, Stem Cell and Brain Research Institute U1208, 69500 Bron, France
[2]Neurogenetics Department, Ecole Pratique des Hautes Etudes, PSL Research University, 75014 Paris, France
[3]Brain Research Institute, University of Zürich/ETHZ, Zürich, Switzerland
[4]Neurocentre Magendie, Neurogenesis and Physiopathology Group, Inserm, U1215, 33077 Bordeaux, France
[5]Université de Bordeaux, 33077 Bordeaux, France
[6]Stem Cell and Brain Research Institute U1208, Université Claude Bernard Lyon 1, Inserm, INRA, USC1361, 69500 Bron, France
[7]Department of Basic Neurosciences, University of Geneva, Geneva, Switzerland
[8]Lead Contact
*Correspondence: v.donega@umcutrecht.nl (V.D.), olivier.raineteau@inserm.fr (O.R.)
https://doi.org/10.1016/j.celrep.2018.02.030

SUMMARY

Progenitors of cortical glutamatergic neurons (*Glu* progenitors) are usually thought to switch fate before birth to produce astrocytes. We used fate-mapping approaches to show that a large fraction of *Glu* progenitors persist in the postnatal forebrain after closure of the cortical neurogenesis period. Postnatal *Glu* progenitors do not accumulate during embryonal development but are produced by embryonal radial glial cells that persist after birth in the dorsal subventricular zone and continue to give rise to cortical neurons, although with low efficiency. Single-cell RNA sequencing reveals a dysregulation of transcriptional programs, which parallels changes in m^{6}A methylation and correlates with the gradual decline in cortical neurogenesis observed *in vivo*. Rescuing experiments show that postnatal progenitors are partially permissive to genetic and pharmacological manipulations. Our study provides an in-depth characterization of postnatal *Glu* progenitors and identifies potential therapeutic targets for promoting brain repair.

INTRODUCTION

During neocortical development, glutamatergic neurons are born from progenitors (*Glu* progenitors) located in the ventricular zone (VZ) and subventricular zone (SVZ) and assemble to form the circuits that underlie cognitive functions. It is classically accepted that the period of cortical neurogenesis closes around embryonic day (E)17.5 in the mouse, with neuronal progenitors switching fate to produce astrocytes (Li et al., 2012).

However, a significant fraction of neural progenitors do not switch fate. For instance, a population of progenitors remain in the postnatal SVZ, contributing to olfactory bulb neurogenesis and parenchymal gliogenesis throughout life (Doetsch et al., 1999). At least some of these progenitors arise from slow-cycling/quiescent embryonal radial glial cells that divide between E13.5 and E15.5 (Fuentealba et al., 2015; Furutachi et al., 2015). Fate-mapping analysis demonstrated that they give rise to distinct neuronal and/or glial lineages, depending on their location in the SVZ (Fiorelli et al., 2015). Surprisingly, several reports suggest the persistence of *Glu* progenitors in the dorsal SVZ (dSVZ) until early adulthood (Brill et al., 2009; Winpenny et al., 2011).

We used Neurog2$^{CreERT2/tdTom}$ mice to permanently and specifically label synchronous cohorts of prenatal and postnatal *Glu* progenitors to study their lineage relationship and transcriptional specificities. Our results show that *Glu* progenitors continue to be produced after closure of the period of cortical neurogenesis. Single-cell RNA sequencing (scRNA-seq) reveals that postnatal *Glu* progenitors show dysregulation in genes involved in metabolism, differentiation, and migration, which parallels a rapid decline in their capacity to migrate and differentiate. Our data suggest that this transcriptional dysregulation in postnatal *Glu* progenitors may result from decreased N^6-methyladenosine (m^{6}A) methylation of certain proneural genes. Nevertheless, postnatal *Glu* progenitors remain partially amenable to pharmacological and genetic manipulations.

RESULTS

Fate Mapping of Birth-Dated Cohorts of Glutamatergic Neurons

The recombination efficiency and specificity of the Neurog2$^{CreERT2/tdTom}$ mice was verified by injecting tamoxifen (Tam) at different embryonal time points (i.e., E13.5 and E15.5) and examining brains after 12 and 24 hr (Figures 1A and 1B). The recombined cells initially expressed the *Glu* progenitor marker, Tbr2, and the proliferation marker Ki67, and rapidly translocated from the VZ to the cortical plate. Fate mapping of

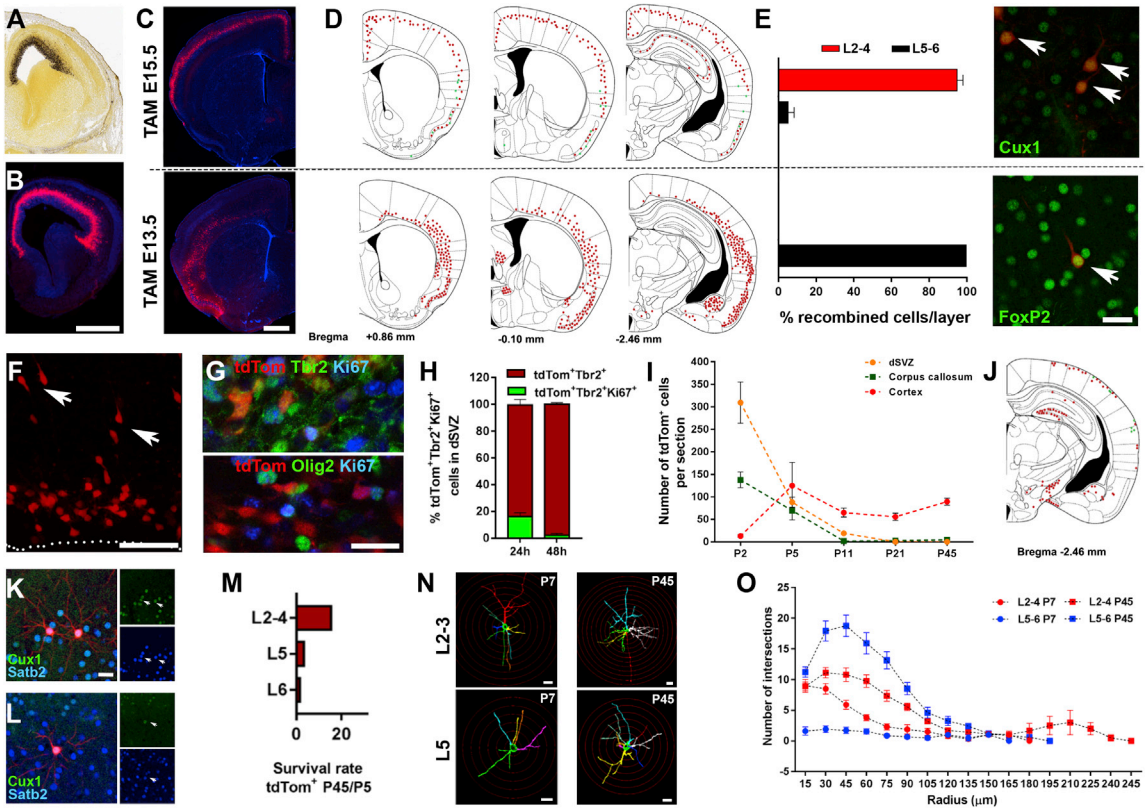

Figure 1. Neurog2$^{CreERT2/tdTom}$ Mice Allow Fate Mapping of Birth-Dated Cohorts of *Glu* Progenitors and Reveal Their Persistence at Postnatal Stages

(A) *In situ* hybridization from the Allen Brain Atlas showing Neurog2 expression in the VZ and SVZ at E15.5.

(B) Specific recombination of *Glu* progenitors in the SVZ following Tam injection at E15.5.

(C and D) Representative coronal sections (C) and drawings illustrating the distribution of recombined neurons at P21 after Tam injection at E13.5 and E15.5 (D).

(E) Immunodetection and quantification of layer marker expression by recombined cortical neurons (see arrows) following Tam at E13.5 and E15.5.

(F) Tam injection at P1 reveals a large population of *Glu* progenitors in the dSVZ (arrows indicate migrating cells) (see also Figures S1 and S2).

(G) Recombined cells express the *Glu* progenitor marker Tbr2 but not Olig2.

(H) Some recombined cells express the proliferative marker Ki67 24 hr post-Tam injection but exit cell cycle by 48 hr.

(I and J) Fate mapping of P0.5 recombined cells at various postnatal time points (I) illustrating the disappearance of recombined cells in the dSVZ, while cortical neuron number increases and stabilizes by P21 (J) (see also Figure S2).

(K and L) High-magnification image showing co-localization of tdTom$^+$ cells with Cux1 and Satb2 (see arrows) in L2–L3 (K) or L5–L6 (L) at P45 (see also Figure S3).

(M–O) Only a fraction of tdTom$^+$ neurons located in upper cortical layer survive at P45 (M), which correlates with their faster maturation (N and O) (see also Figure S4).

TAM, tamoxifen. Scale bars: 500 μm in (B); 1,000 μm in (C); 50 μm in (F); 25 μm in (E), (G), (K), and (L); and 20 μm in (N). Data are presented as mean ± SEM. See also Figures S1, S2, S3, and S4.

recombined cells was assessed at postnatal day (P)21. Tam injections at either E13.5, E15.5, or E17.5 labeled neurons in subcortical and cortical brain regions in accordance with their date of birth (Figure S1). To confirm the precise labeling of birth-dated cohorts of glutamatergic neurons, we performed a more detailed analysis of recombined cells in the cortex. Tam injection at E13.5 labeled neurons in the deep cortical layers (i.e., L5–L6), which expressed the deep cortical layer marker FoxP2, (Figures 1C–1E). In contrast, recombination at E15.5 labeled neurons in L3–L4, which expressed the upper layer marker Cux1 (Figures 1C–1E). Importantly, only a few glial-like cells were labeled (<1% of total tdTom$^+$ cells) from E15.5 on. These glial cells were found in clusters, suggesting that only a very limited number of progenitors switched from a glutamatergic to an astrocytic fate (Figure S1). Altogether, these observations confirm that Neurog2$^{CreERT2/tdTom}$ mice allow the specific labeling of birth-dated cohorts of glutamatergic neurons.

A Large Population of *Glu* Progenitors Persist in the Postnatal SVZ

Having established the lineage and temporal specificity of recombination in the Neurog2$^{CreERT2/tdTom}$ mice, we performed Tam injections in postnatal mice. Recombination at P0.5 revealed that a large pool of *Glu* progenitors persist in the early postnatal dSVZ and subcallosal zone (SCZ), despite closure of the cortical neurogenic period (Figure 1F; Figure S2A). Recombined cells were confirmed to be *Glu* progenitors by their expression of Tbr2 (Figure 1G) but exclusion of other lineage

markers (e.g., Olig2). Twenty-four hours following recombination, ~20% of *Glu* progenitors were still actively cycling, but most had exited the cell cycle by P3 (Figure 1H). To follow the long-term fate of these progenitors, we injected Tam in P0.5 pups and sacrificed them at various time points. At P2, most recombined cells were observed in the dSVZ, but their number gradually decreased with age, disappearing by P21 (Figure 1I). In parallel, *Glu* progenitors gave rise to a cohort of migrating neurons that transiently increased in the corpus callosum and cingulum, as they left the dSVZ and migrated toward the cortex (Figures 1I and 1J). At P21, tdTom$^+$ neurons were observed in the cortex, in the dentate gyrus, and in some subcortical nuclei (Figure 1J; Figure S2B). The number of recombined cortical neurons increased from frontal to caudal brain sections (Figure S2C), with most neurons located in sensory rather than motor regions (Figure S2D). A marked decrease in the number of recombined neurons was observed over time. Indeed, comparison of the number of tdTom$^+$ cells at short and long survival times (i.e., 12 hr post-Tam injection or at P21, respectively), revealed a large decrease (81.3%) following a P0.5 Tam injection. In comparison, a marginal drop was observed in the number of cells recombined at E15.5 (11.8%), indicating that while most recombined embryonal progenitors produce neurons that efficiently survive until P21, only a fraction do so at postnatal time points.

We next looked in more detail at the location and phenotype of recombined cortical neurons. Most recombined glutamatergic neurons were located in upper cortical layers L2–L3, and a few were located in L5–L6 (Figures S3A–S3D). By P45, most recombined neurons expressed the marker Satb2. While recombined neurons located in L2–L3 also expressed the upper layer marker Cux1, those in L5–L6 did not express the markers of deep cortical layers, Ctip2 or FoxP2 (Figures 1K and 1L; Figure S3E). By P45, the decrease in number of recombined neurons was more pronounced in deeper cortical layers than in superficial layers (Figure 1M), as around 1% of the total number of tdTom$^+$ neurons were located in L5–L6 (i.e., 30–48 cells per brain). This decreased survival correlated with a slower maturation of surviving neurons in deep cortical layers (Figures 1N and 1O). Nevertheless, surviving glutamatergic neurons of both upper and deep layers developed spines (Figure S4A), thereby suggesting proper integration of newborn glutamatergic neurons. In contrast to neurons produced at E13.5, which formed corticofugal (i.e., internal capsule or corticospinal) projections, postnatally born neurons only formed intracortical projections, as shown by the presence of axons in the corpus callosum (Figure S4B). Taken together, these results reveal that closure of the cortical neurogenic period is not due to the disappearance of *Glu* progenitors but rather to a gradual decline in their capacity to differentiate and survive.

ScRNA-Seq Reveals Transcriptional Dysregulation in Postnatal *Glu* Progenitors

We next investigated the origin and transcriptional specificities of postnatal *Glu* progenitors. Injection of Tam at E13.5 or E15.5 failed to label *Glu* progenitors at P2 (Figures 2A–2F). In contrast, *in utero* electroporation of a transposon-GFP plasmid (Siddiqi et al., 2014) at either E13.5 or E15.5 revealed a large pool of GFP$^+$ cells that persisted in the postnatal dSVZ and continued generating proliferating Tbr2$^+$ cells at P2 (Figures 2G and 2H) as well as at P21 (Figures 2I and 2J). Together, these results indicate that postnatal *Glu* progenitors do not accumulate during embryonic development but are produced by embryonic radial glial cells (RGCs) that persist after birth in the dSVZ, in accordance with recent studies (Fuentealba et al., 2015; Furutachi et al., 2015). To explore the mechanisms of the decreased neurogenic capacity of postnatal *Glu* progenitors, we performed scRNA-seq of tdTom$^+$ cells isolated by flow cytometry from microdissected pallium at E15.5 or P2. Unbiased clustering combined with interrogation of cell-cycle and post-mitotic markers revealed several cell clusters (Figures 3A and 3B), corresponding to actively cycling recombined cells (i.e., *progenitors*) and their immediate progeny (i.e., *nascent neurons*) (Figure 3B). Expression of lineage-specific transcripts, such as Neurog2 and Tbr2, confirmed their *Glu* identity (Figure 3C). Transcriptional differences increased during differentiation, with 597 (8%) and 1.425 (20%) genes being differentially regulated between E15.5 and P2 *progenitors* and *nascent neurons*, respectively (Figures 3D and 3E; Table S1; see https://genebrowser.lyon.inserm.fr/ for an interactive dataset). Thus, while the vast majority (~90%) of E15.5 top 1,000 expressed genes were also expressed in P2 *progenitors*, only 40% of the E15.5 top 1,000 genes were similarly expressed in *nascent neurons* at P2 (Figure 3F). Interestingly, transcripts enriched in *Glu progenitors* (i.e., *Sox2*, *Pax6*, *Neurog2*, and *Tbr2*) were upregulated at P2, suggesting a transcriptional dysregulation leading to the persistence of progenitor traits in *nascent neurons* (Figure 3G). Knowing that m^{6}A methylation plays a role in cortical neurogenesis by regulating the expression of proneural transcripts (Yoon et al., 2017), we assessed whether this mRNA modification was decreased in postnatal *Glu* progenitors. Transcriptional analysis confirmed a downregulation of transcripts coding for proteins of the methyltransferase complex, Mettl3 and Mettl14 (Figure 3G), while expression of *YTHDF2*, which has been shown to localize m^{6}A-tagged transcripts to decay sites (Wang et al., 2015), was not changed (data not shown). To assess m^{6}A methylation level in *Glu* progenitors, we performed an mRNA dot blot assay to detect m^{6}A modifications (Figures 3H and 3I). Our results reveal a 65% decrease in m^{6}A level in the postnatal dSVZ, compared to the E15.5 pallium. All together, these data suggest that epitranscriptomic modifications participate in the transcriptional dysregulation observed in postnatal *Glu* progenitors and their immediate progeny.

Postnatal *Glu* Progenitor Differentiation Can Be Partially Rescued

We next focused on the transcriptional specificities of P2 *Glu progenitors* and *nascent neurons*. Classification of transcripts differentially expressed in *Glu* progenitors highlighted depressed transcriptional and metabolic activities at P2 that correlates with reduced potential of *Glu* progenitors to differentiate postnatally (Figure 3J). Classification of differentially expressed transcripts in *nascent neurons* highlighted downregulation of generic programs of differentiation and migration, and an upregulation of genes involved in neuronal death (Figure 3K), in line with our histological observations. A KEGG analysis further highlighted

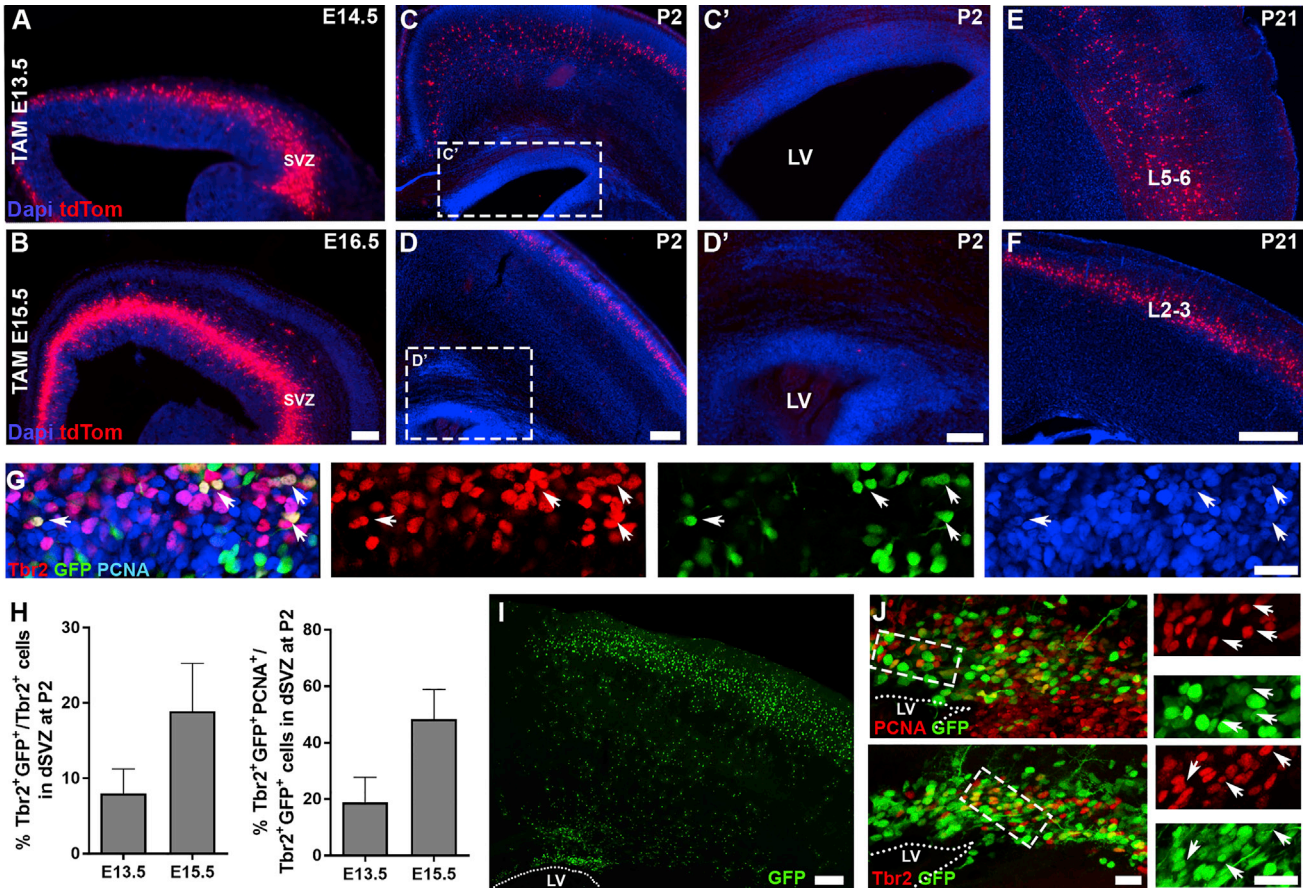

Figure 2. Postnatal *Glu* Progenitors Originate from a Pool of Slow-Cycling RGCs that Accumulate in the SVZ during Corticogenesis

(A–F) tdTom$^+$ cells recombined at embryonal time points do not remain in the postnatal dSVZ (C–D') but generate the different *Glu* projection neurons embryonally. tdTom$^+$ cells in the pallium 24 hr after TAM injection (A and B) and at P2 or P21 in L5–L6 (C and E) or L2–L3 (D and F) are indicated.

(G–J) In utero electroporation (IUE) of transposon-GFP in the pallium at embryonal time points E13.5 (G) and E15.5 (I and J) highlight persisting RGCs (see arrows) in the dSVZ that continue giving rise to proliferating Tbr2$^+$ cells at P2 (G and H) as well as at the later postnatal time point P21 (in I and J).

Scale bars: 500 μm in (E) and (F); 200 μm in (C), (D), and (I); 100 μm in (A), (B), (C'), and (D'); and 25 μm in (G) and (J). Data are presented as mean ± SEM.

paralleled perturbation of several key signaling pathways, such as Wnt canonical signaling (Figure 3L), as previously suggested (Li et al., 2012). A more detailed analysis into downregulated GO terms, revealed a decrease in several genes, including *Ctnnb1* (i.e., β-*catenin*) and other Wnt signaling transcripts such as, *Fzd1* and *Lef1* (Figures 4A and 4B). Protein-protein interaction (PPI) analysis further emphasized the central role of β-*catenin*, as most of the downregulated genes at P2 encode for proteins that interact with it (Figure 4C). To assess if migration and differentiation of postnatal *Glu* progenitors could be reactivated, we performed experiments to rescue downregulated signaling and transcriptional pathways. We first used a glycogen synthase kinase 3β (GSK3β) inhibitor, AR-A014418, to activate the canonical Wnt signaling pathway. Our results showed increased tdTom$^+$ cells in the dSVZ, which was paralleled by increased proliferation (Figures 4D–4F). Next, we selected *Bcl11a* as a candidate gene for overexpression, as this transcription factor is among the top 10 differentially expressed (i.e., downregulated) transcription factors at P2 (Figure 4G). *Bcl11a* has been shown to regulate both migration and fate specification during embryonic development (Wiegreffe et al., 2015; Greig et al., 2016). Overexpression of *Bcl11a* increased proliferation in the dSVZ (Figure 4H). In addition, our results show a significant increase in migration towards the cortex and increased number of cells that adopted bipolar morphologies (Figures 4H–4J). Together, these results demonstrate that *Glu* progenitors remain permissive to both pharmacological and genetic manipulation.

DISCUSSION

Our work highlights the persistence of a large population of *Glu* progenitors in the postnatal forebrain, after the closure of the cortical neurogenic period. Fate mapping and scRNA-seq reveal a dysregulation of transcriptional and signaling pathways that contribute to restricting the neurogenic potential of postnatal *Glu* progenitors early after birth. Rescuing experiments, however, show that postnatal progenitors remain partially permissive to genetic and pharmacological manipulations, suggesting that they could be recruited for cortical repair.

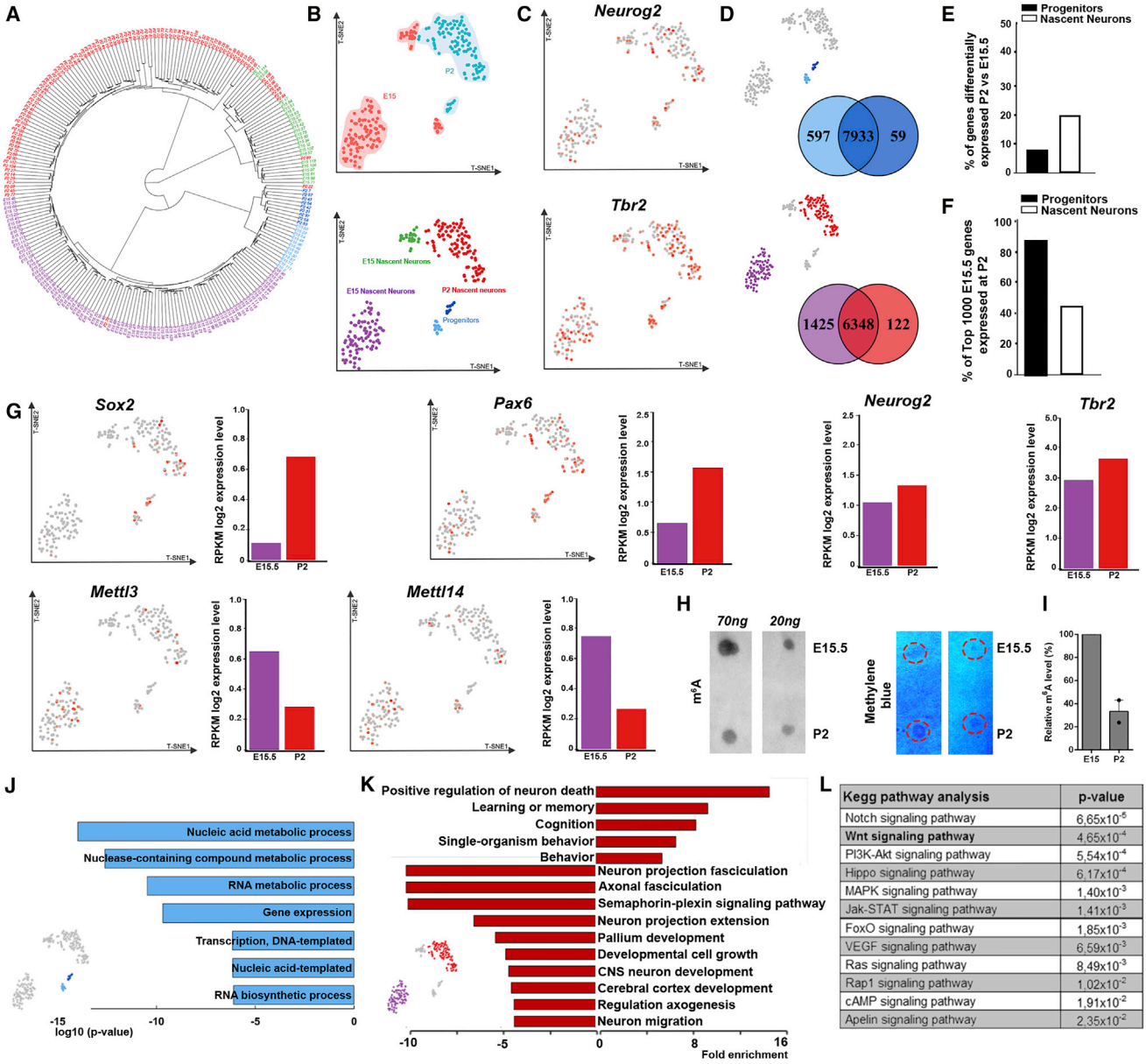

Kegg pathway analysis	p-value
Notch signaling pathway	$6{,}65\times10^{-5}$
Wnt signaling pathway	$4{,}65\times10^{-4}$
PI3K-Akt signaling pathway	$5{,}54\times10^{-4}$
Hippo signaling pathway	$6{,}17\times10^{-4}$
MAPK signaling pathway	$1{,}40\times10^{-3}$
Jak-STAT signaling pathway	$1{,}41\times10^{-3}$
FoxO signaling pathway	$1{,}85\times10^{-3}$
VEGF signaling pathway	$6{,}59\times10^{-3}$
Ras signaling pathway	$8{,}49\times10^{-3}$
Rap1 signaling pathway	$1{,}02\times10^{-2}$
cAMP signaling pathway	$1{,}91\times10^{-2}$
Apelin signaling pathway	$2{,}35\times10^{-2}$

Figure 3. Dysregulation of Neurogenic Transcriptional Coding in Postnatal *Glu* Progenitors

(A and B) Hierarchical clustering (A) and t-SNE of individual cells recombined at E15.5 and P2 allows distinguishing 2 clusters of cells, actively cycling cells (i.e., progenitors), and their immediate progeny (i.e., nascent neurons) (B).

(C) Feature plot showing the expression of transcripts of the *Glu* lineage.

(D) Venn diagrams showing the number of differentially expressed transcripts in *progenitors* or *nascent neurons*.

(E and F) Transcriptional differences increase as differentiation progresses, as reflected by the percentage of transcripts differentially expressed between E15.5 and P2 (E), as well as the gradual loss of transcripts expressed at E15.5 in P2-sorted cells (F).

(G) Feature plots showing downregulation of methyltransferases *Mettl3* and *Mettl14* in P2 progenitors and upregulation of m^6A-tagged transcripts *Sox2*, *Pax6*, *Neurog2*, and *Tbr2*.

(H) Dot blot showing decreased m^6A levels at P2 and methylene blue staining confirming equal mRNA loading on membrane.

(I) Quantification of m^6A levels.

(J) GO showing downregulation in P2 *progenitors* of transcripts involved in transcription and metabolism.

(K) GO analysis showing downregulation of migration, differentiation, and cell death in P2 *nascent neurons*.

(L) KEGG pathway analysis highlighting dysfunctional signaling pathways.

Data are presented as mean ± SEM.

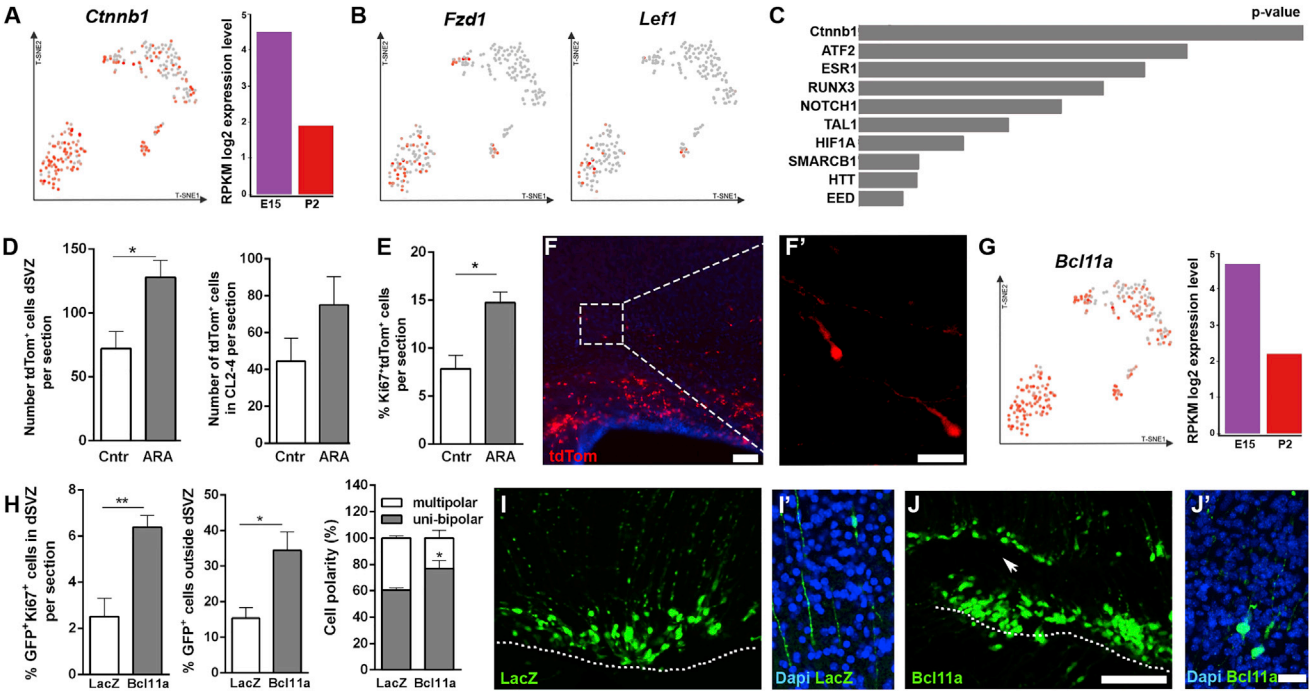

Figure 4. Partial Rescue of Impaired Migration and Differentiation of Postnatal *Glu* Progenitors by Pharmacological and Genetic Manipulations

(A) Feature plot showing decreased expression *Ctnnb1* (*β-catenin*) in P2 *nascent neurons*.

(B) Feature plots showing altered expression of two Wnt-signaling transcripts.

(C) PPI analysis showing the top 10 proteins to interact with proteins coded by genes downregulated at P2.

(D–F') Pharmacological activation of the Wnt canonical pathway increases the (D) number and (E) proliferation (Ki67) of tdTom$^+$ cells in the dSVZ at 72 hr. (F and F') Representative images showing tdTom$^+$ progenitors migrating away from the dSVZ.

(G) Feature plot showing decreased expression of *Bcl11a* in P2 *nascent neurons*.

(H) Overexpression of *Bcl11a* increases proliferation in the dSVZ while promoting cell migration and bipolar cell morphology outside the dSVZ.

(I–J') Representative images after electroporation of control plasmid (LacZ) (I–I') or *Bcl11a* (J–J') overexpression.

Scale bars: 100 μm in (F); 50 μm in (J); and 25 μm in (F') and (J'). *p < 0.05; **p < 0.005. Data are presented as mean ± SEM.

The perinatal period has long been considered as a period of exclusive cortical gliogenesis associated with the maturation of embryonically born neurons into functional circuits. This view is currently challenged by the demonstration of neurogenesis in specific cortical regions. Thus, GABAergic progenitors accumulate in the early postnatal white matter and give rise to a subpopulation of cortical interstitial interneurons (Frazer et al., 2017). In addition, the migration of interneurons into the frontal cortex has been shown to persist early after birth in rodents (Inta et al., 2008; Le Magueresse et al., 2012), as well as in human babies (Paredes et al., 2016). Our results reveal that this persisting neurogenesis is not restricted to the GABAergic lineage but also includes neurons of the glutamatergic lineage. Indeed, our work identifies a small population of cortical Satb2/Cux1$^+$ neurons that are generated at birth. Surviving neurons develop spines and intracortical axonal projections, supporting their integration into cortical networks. Our results further indicate that these neurons arise from a large population of pallial RGCs that do not switch fate toward astrogenesis and persist in the dSVZ. These results are in line with recent mosaic analysis with double markers (MADM) experiments suggesting that only 1 out of 6 neurogenic RGCs produce glia (Gao et al., 2014).

Our results underline a rapid decline in the capacity of *Glu* progenitors to differentiate and migrate, thereby contributing to the closure of the period of cortical neurogenesis. Our scRNA-seq data shed light on the mechanisms mediating this gradual loss of neurogenic potency. Epitranscriptomic changes are emerging as key mechanisms in mediating temporal control over lineage progression. m^{6}A is the most prevalent mRNA modification in eukaryotic cells (Desrosiers et al., 1975) and has recently been suggested to regulate transcriptional prepatterning during corticogenesis (Yoon et al., 2017). Our results identify m^{6}A methylation as a possible mechanism leading to the transcriptional dysregulation that we observe in postnatal *Glu* progenitors. In addition to these epitranscriptomic modifications, KEGG pathway analysis highlights changes in several key signaling pathways, such as those involved in astrogenesis (i.e., Jak-Stat and Notch signaling pathways; Rowitch and Kriegstein, 2010), suggesting that they may concomitantly affect the differentiation potential of *Glu* progenitors. Another signaling pathway that is dysregulated is the Wnt signaling pathway. This is in agreement with a previous study describing a gradual increase in GSK3β activity from E15.5 on, which results in the phosphorylation of Neurog2, thereby affecting its activity

(Li et al., 2012). In line with a decreased transcriptional activity of Neurog2, 64% of its target genes (Gohlke et al., 2008) are downregulated at P2, while only 2% are upregulated, despite the persistence of Neurog2 expression.

Importantly, postnatal *Glu* progenitors appear to be still permissive to intrinsic/extrinsic manipulation. We show that proliferation and migration of postnatal *Glu* progenitors can be promoted by genetic or pharmacological manipulations. Our experiments, however, reveal that these manipulations are not sufficient for promoting long-term neuron survival, suggesting that the cortex is not permissive to the integration of these newborn neurons under physiological conditions. However, recent observations suggest that permissiveness of the environment might be increased following injury, such as after neonatal chronic hypoxia, where cortical *de novo* neurogenesis has been observed (Fagel et al., 2009; Bi et al., 2011; Falkner et al., 2016; Azim et al., 2017). It is likely that our results will provide important information to guide future research in this context.

EXPERIMENTAL PROCEDURES

Further details can be found in the Supplemental Experimental Procedures.

Ethical Statement

All animal experiments were performed in accordance with international guidelines from the EU directive 2012/63/EU and approved by the Animal Care and Use Committee CELYNE (APAFIS#187 & #188).

Animals

The Neurog2^{CreERT2} transgenic mouse line was crossed with the reporter line Rosa^{tdTomato} (tdTom) (Madisen et al., 2010), allowing the specific labeling of *Glu* progenitors and their immediate progeny. For fate mapping of birth-dated cohorts of *Glu* progenitors, tamoxifen was administered to Neurog2$^{CreERT2/tdTom}$ transgenic mice at various embryonal and postnatal time points. The morning when a plug was observed was considered as E0.5, and the day of birth was defined as P0.

In Utero Electroporation

In utero electroporation was performed at E13.5 or E15.5 to investigate the embryonal origin of postnatal *Glu* progenitors, using a mixture of transposon pPB-EBFP-P2A-GFP and hyperactive piggyBac transposase.

Immunohistochemistry

Animals were sacrificed with an overdose of pentobarbital and fixed by transcardial perfusion with PBS followed by 4% paraformaldehyde (PFA; w/v). Brains were dissected and post-fixed in 4% PFA at 4°C. Free-floating vibratome serial sections were cut at a thickness of 50 μm. Immunostainings were performed as described previously.

Quantifications

Images were taken on a Leica SPE confocal laser microscope using 10×/0.3 NA, 20×/0.75 NA, or 40×/1.25 NA oil objectives (HCPL Fluotar) and the software LAS (Leica Microsystems, v3.1.2.16221). Quantifications were performed on coronal sections by counting the number of cells either by eye from confocal images or from z stack mosaic images of the entire dSVZ on ImageJ. Depending on the analysis, quantifications were done either on an entire series of sections or on at least 3 equally spaced sections of the SVZ. Images for Sholl analysis were taken with a z-step of 0.29 μm and a resolution of 1,024 × 1,024. Sholl analysis was performed on Neurolucida 360 software (MBF Bioscience). Images were processed using Photoshop (CC2015.5, Adobe Systems Software).

Single-Cell Capture, cDNA Library Preparation, and Sequencing

The brains of E15 and P2 mice were harvested and placed on ice-cold Hank's balanced salt solution (HBSS) for microdissection. A total of 230 cells were obtained (121 at E15.5 and 109 at P2). Reverse transcription and pre-amplification of the single-cell cDNAs were done within the integrated fluidic circuit (IFC) chip using the SMARTer Ultra Low RNA kit for Illumina (Clontech) according to the C1 protocol. Upon termination of the run, amplified cDNA was harvested, and the concentration of cDNA was assessed on a SpectraMax Gemini Fluorimeter (Molecular Devices). RNA-seq libraries of the harvested cDNA were prepared using the Illumina Nextera XT DNA Sample Preparation Kit. Libraries were muliplexed and sequenced using the Illumina HiSEQ500 platform.

m^{6}A Dot Blot Assay

The pallium and dSVZ were isolated (n = 4) at E15.5 and P2, respectively. mRNA was harvested using the Dynabeads mRNA Direct Purification Kit (61011, Thermo Fisher, Waltham, MA, USA). 20 ng mRNA per 1 μL was applied to an Amersham Hybond-N$^+$ membrane (Amersham, Buckinghamshire, UK). m^{6}A was detected by incubating with primary antibody m^{6}A (mouse, 1:500, 212B11 Synaptic Systems, Goettingen, Germany) followed by secondary antibody enhanced chemiluminescence (ECL) horseradish peroxidase (HRP)-conjugated (sheep-anti-mouse, 1:5,000, Amersham). Signal was visualized using the Supersignal West Femto Maximum Sensitivity Substrate (34096, Thermo Scientific).

Pharmacological Activation of the Canonical Wnt Signaling Pathway

Activation of the Wnt/β-catenin pathway was done by intraperitoneal injections of the GSK3β inhibitor, AR-A014418 (Sigma-Aldrich, A3230) (Azim et al., 2014).

Bcl11a Gain of Function

Bcl11a and control LacZ plasmids were obtained from VectorBuilder (Neu-Isenburg, Germany). Electroporation of the dSVZ was performed as described previously (Fernández et al., 2011).

Statistical Analysis

Data are expressed as mean ± SEM (n ≥ 3). Significance was tested on GraphPad Prism 7 by using an unpaired t test or 2-way ANOVA followed by Bonferroni post hoc test.

Data and Software Accessibility

The accession numbers for the data reported in this paper are GEO: GSE109556 and have been posted to Mendeley at https://doi.org/10.17632/k659jr9gvv.1.

SUPPLEMENTAL INFORMATION

Supplemental Information includes Supplemental Experimental Procedures, four figures, and two tables and can be found with this article online at https://doi.org/10.1016/j.celrep.2018.02.030.

ACKNOWLEDGMENTS

We are grateful to Arthur Butt for critical reading of the manuscript, as well as to Ludovic Telley for guidance in performing the single-cell RNA-seq analysis and I. Durand (CRCL, Lyon) for her advice regarding cell sorting. We thank A. Simon, D. Frasheri, and R. Kaestli for their help in setting up the histological mapping; J. Lachuer, C. Rey, and S. Croze (genomic platform ProfilXpert, Lyon) for their expert help with C1 single-cell RNA-seq; and B. Smatti (imaging platform CiQle, Lyon) for her guidance in using the slide scanner. This work was supported by a grant from the "Programme Avenir Lyon Saint-Etienne." V.D. was supported by grants from IRME ("Institut pour la Recherche sur la Moelle épinière et l'Encéphale") and from the FRC ("Fédération pour la Recherche sur le Cerveau"), and G.M. was supported by a PhD fellowship from the Labex Cortex.

AUTHOR CONTRIBUTIONS

Conceptualization, O.R. and V.D.; Methodology, O.R.; Software, Q.L.G. and D.J.; Investigation, V.D., G.M., S.Z., D.A., R.F., S.R.-G., and M.K.; Writing – Original Draft, V.D., G.M., and O.R.; Writing – Review and Editing, V.D., G.M., and O.R.; Visualization, V.D., G.M., and O.R.; Supervision, O.R., D.N.A., V.D., and G.M.; Funding Acquisition, O.R. and V.D.

DECLARATION OF INTERESTS

The authors declare no competing interests.

Received: September 15, 2017
Revised: December 22, 2017
Accepted: February 7, 2018
Published: March 6, 2018

REFERENCES

Azim, K., Fischer, B., Hurtado-Chong, A., Draganova, K., Cantù, C., Zemke, M., Sommer, L., Butt, A., and Raineteau, O. (2014). Persistent Wnt/β-catenin signaling determines dorsalization of the postnatal subventricular zone and neural stem cell specification into oligodendrocytes and glutamatergic neurons. Stem Cells *32*, 1301–1312.

Azim, K., Angonin, D., Marcy, G., Pieropan, F., Rivera, A., Donega, V., Cantù, C., Williams, G., Berninger, B., Butt, A.M., and Raineteau, O. (2017). Pharmacogenomic identification of small molecules for lineage specific manipulation of subventricular zone germinal activity. PLoS Biol. *15*, e2000698.

Bi, B., Salmaso, N., Komitova, M., Simonini, M.V., Silbereis, J., Cheng, E., Kim, J., Luft, S., Ment, L.R., Horvath, T.L., et al. (2011). Cortical glial fibrillary acidic protein-positive cells generate neurons after perinatal hypoxic injury. J. Neurosci. *31*, 9205–9221.

Brill, M.S., Ninkovic, J., Winpenny, E., Hodge, R.D., Ozen, I., Yang, R., Lepier, A., Gascón, S., Erdelyi, F., Szabo, G., et al. (2009). Adult generation of glutamatergic olfactory bulb interneurons. Nat. Neurosci. *12*, 1524–1533.

Desrosiers, R.C., Friderici, K.H., and Rottman, F.M. (1975). Characterization of Novikoff hepatoma mRNA methylation and heterogeneity in the methylated 5′ terminus. Biochemistry *14*, 4367–4374.

Doetsch, F., Caillé, I., Lim, D.A., García-Verdugo, J.M., and Alvarez-Buylla, A. (1999). Subventricular zone astrocytes are neural stem cells in the adult mammalian brain. Cell *97*, 703–716.

Fagel, D.M., Ganat, Y., Cheng, E., Silbereis, J., Ohkubo, Y., Ment, L.R., and Vaccarino, F.M. (2009). Fgfr1 is required for cortical regeneration and repair after perinatal hypoxia. J. Neurosci. *29*, 1202–1211.

Falkner, S., Grade, S., Dimou, L., Conzelmann, K.K., Bonhoeffer, T., Götz, M., and Hübener, M. (2016). Transplanted embryonic neurons integrate into adult neocortical circuits. Nature *539*, 248–253.

Fernández, M.E., Croce, S., Boutin, C., Cremer, H., and Raineteau, O. (2011). Targeted electroporation of defined lateral ventricular walls: a novel and rapid method to study fate specification during postnatal forebrain neurogenesis. Neural Dev. *6*, 13.

Fiorelli, R., Azim, K., Fischer, B., and Raineteau, O. (2015). Adding a spatial dimension to postnatal ventricular-subventricular zone neurogenesis. Development *142*, 2109–2120.

Frazer, S., Prados, J., Niquille, M., Cadilhac, C., Markopoulos, F., Gomez, L., Tomasello, U., Telley, L., Holtmaat, A., Jabaudon, D., and Dayer, A. (2017). Transcriptomic and anatomic parcellation of 5-HT3AR expressing cortical interneuron subtypes revealed by single-cell RNA sequencing. Nat. Commun. *8*, 14219.

Fuentealba, L.C., Rompani, S.B., Parraguez, J.I., Obernier, K., Romero, R., Cepko, C.L., and Alvarez-Buylla, A. (2015). Embryonal origin of postnatal neural stem cells. Cell *161*, 1644–1655.

Furutachi, S., Miya, H., Watanabe, T., Kawai, H., Yamasaki, N., Harada, Y., Imayoshi, I., Nelson, M., Nakayama, K.I., Hirabayashi, Y., and Gotoh, Y. (2015). Slowly dividing neural progenitors are an embryonic origin of adult neural stem cells. Nat. Neurosci. *18*, 657–665.

Gao, P., Postiglione, M.P., Krieger, T.G., Hernandez, L., Wang, C., Han, Z., Streicher, C., Papusheva, E., Insolera, R., Chugh, K., et al. (2014). Deterministic progenitor behavior and unitary production of neurons in the neocortex. Cell *159*, 775–788.

Gohlke, J.M., Armant, O., Parham, F.M., Smith, M.V., Zimmer, C., Castro, D.S., Nguyen, L., Parker, J.S., Gradwohl, G., Portier, C.J., and Guillemot, F. (2008). Characterization of the proneural gene regulatory network during mouse telencephalon development. BMC Biol. *6*, 15.

Greig, L.C., Woodworth, M.B., Greppi, C., and Macklis, J.D. (2016). Ctip1 controls acquisition of sensory area identity and establishment of sensory input fields in the developing neocortex. (2016). Neuron *90*, 261–277.

Inta, D., Alfonso, J., von Engelhardt, J., Kreuzberg, M.M., Meyer, A.H., van Hooft, J.A., and Monyer, H. (2008). Neurogenesis and widespread forebrain migration of distinct GABAergic neurons from the postnatal subventricular zone. Proc. Natl. Acad. Sci. USA *105*, 20994–20999.

Le Magueresse, C., Alfonso, J., Bark, C., Eliava, M., Khrulev, S., and Monyer, H. (2012). Subventricular zone-derived neuroblasts use vasculature as a scaffold to migrate radially to the cortex in neonatal mice. Cereb. Cortex *22*, 2285–2296.

Li, S., Mattar, P., Zinyk, D., Singh, K., Chaturvedi, C.P., Kovach, C., Dixit, R., Kurrasch, D.M., Ma, Y.C., Chan, J.A., et al. (2012). GSK3 temporally regulates neurogenin 2 proneural activity in the neocortex. J. Neurosci. *32*, 7791–7805.

Madisen, L., Zwingman, T.A., Sunkin, S.M., Oh, S.W., Zariwala, H.A., Gu, H., Ng, L.L., Palmiter, R.D., Hawrylycz, M.J., Jones, A.R., et al. (2010). A robust and high-throughput Cre reporting and characterization system for the whole mouse brain. Nat. Neurosci. *13*, 133–140.

Paredes, M.F., James, D., Gil-Perotin, S., Kim, H., Cotter, J.A., Ng, C., Sandoval, K., Rowitch, D.H., Xu, D., McQuillen, P.S., et al. (2016). Extensive migration of young neurons into the infant human frontal lobe. Science *354*, aaf5053.

Rowitch, D.H., and Kriegstein, A.R. (2010). Developmental genetics of vertebrate glial-cell specification. Nature *468*, 214–222.

Siddiqi, F., Chen, F., Aron, A.W., Fiondella, C.G., Patel, K., and LoTurco, J.J. (2014). Fate mapping by piggyBac transposase reveals that neocortical GLAST+ progenitors generate more astrocytes than Nestin+ progenitors in rat neocortex. Cereb. Cortex *24*, 508–520.

Wang, X., Zhao, B.S., Roundtree, I.A., Lu, Z., Han, D., Ma, H., Weng, X., Chen, K., Shi, H., and He, C. (2015). N^6-methyladenosine modulates messenger RNA translation efficiency. Cell *161*, 1388–1399.

Wiegreffe, C., Simon, R., Peschkes, K., Kling, C., Strehle, M., Cheng, J., Srivatsa, S., Liu, P., Jenkins, N.A., Copeland, N.G., et al. (2015). Bcl11a (Ctip1) controls migration of cortical projection neurons through regulation of Sema3c. Neuron *87*, 311–325.

Winpenny, E., Lebel-Potter, M., Fernandez, M.E., Brill, M.S., Götz, M., Guillemot, F., and Raineteau, O. (2011). Sequential generation of olfactory bulb glutamatergic neurons by Neurog2-expressing precursor cells. Neural Dev. *6*, 12.

Yoon, K.J., Ringeling, F.R., Vissers, C., Jacob, F., Pokrass, M., Jimenez-Cyrus, D., Su, Y., Kim, N.S., Zhu, Y., Zheng, L., et al. (2017). Temporal control of mammalian cortical neurogenesis by m^6A methylation. Cell *171*, 877–889.e17.